Supplementary Information to

Regulation of cerebral metabolism during cortical spreading depression

Authors:
D. Feuerstein[1]†, H. Backes[1]†*, M. Gramer[1], M. Takagaki[2], P. Gabel[1], T. Kumagai[2], R. Graf[1]

Affiliations:

[1] Max Planck Institute for Metabolism Research, Cologne, Germany.

[2] Department of Neurosurgery, Osaka University Graduate School of Medicine, 2-2 Yamadaoka, Japan.

*Correspondence to: backes@nf.mpg.de
†These authors contributed equally to this work.

Supplemental Material S1 - Two-cell type model

Model equations and assumptions

In the face of substrate kinetics brain tissue was considered to be effectively composed of two cell types, neurons and astrocytes, which are supplied with glucose by the local blood flow (Fig. 2a). The volume fraction of astrocytes of the total cellular volume was taken as $r_a = 0.36$ according to Mangia et al. JCBFM 2011 [1]. Brain tissue was supplied by $C_p = 4.4$ mM glucose (average value of plasma glucose under propofol anesthesia for n=15 animals). All concentrations used in this model are in relation to tissue volume. Glucose and lactate can enter and leave a volume of tissue. The amounts of glucose and lactate that enter brain tissue per time are given as fractions of C_P: $K_1 C_P$ for glucose and $k_{PL} C_P$ for lactate. Within the tissue they can have several forms or compartments, while the model accounts for mass-conservation during transitions between the compartments:

- Extracellular glucose, C_E, considered in equilibrium with free intracellular glucose [2]
- Intracellular metabolized glucose, C_{aM} and C_{nM} for astrocytes and neurons respectively. In both cell types, metabolized glucose represents the precursor pool for either oxidative ATP production in the TCA cycle, or lactate or glycogen production.
- Intracellular glycogen in astrocytes: C_G
- Intracellular ATP concentrations (C_{aATP} and C_{nATP}) the fate of glucose would be CO_2 in this case)
- Extracellular lactate, C_L, given that 2 molecules of lactate are produced per molecule of glucose.

All steps in glucose metabolism, from transport through the blood-brain barrier to complete oxidative phosphorylation are assumed to follow first-order kinetics, characterized by constants k:

– K_1 and k_2 quantify the transport rate of glucose from blood to brain and from brain to blood respectively

– k_3 is the rate constant for phosphorylation of brain glucose by hexokinase. The astrocyte:neuron volume ratio determines the respective rate constants for astrocytes and neurons k_{a3} and k_{n3}: $k_3 = r_a\, k_{a3} + (1\text{-}r_a)\, k_{n3}$.

– k_{aOXY} and k_{nOXY} are the rate constants for the full oxidation of metabolized glucose by mitochondria in astrocytes and neurons respectively.

– all intermediary steps in glucose metabolism from compartment U to compartment V are characterized by the rate constant k_{aUV} and k_{nUV} for astrocytes and neurons respectively.

Accordingly, the concentration changes for each compartment are given by the following time-dependent equations:

$$\frac{dC_E}{dt} = K_1 C_P - (k_2 + k_{n3} + k_{a3}) C_E \quad (1)$$

$$\frac{dC_{nM}}{dt} = k_{n3} C_E - (k_{nML} + k_{nOXY}) C_{nM} + k_{nLM} C_L \quad (2)$$

$$\frac{dC_{aM}}{dt} = k_{a3} C_E - (k_{aML} + k_{aOXY} + k_{MG}) C_{aM} + k_{aLM} C_L + k_{GM} C_G \quad (3)$$

$$\frac{dC_L}{dt} = k_{PL} C_P + k_{nML} C_{nM} + k_{aML} C_{aM} - (k_{nLM} + k_{aLM} + k_{LP}) C_L \quad (4)$$

$$\frac{dC_G}{dt} = k_{MG} C_{aM} - k_{GM} C_G \quad (5)$$

$$\frac{dC_{nATP}}{dt} = 2k_{n3} C_E + 29 k_{nOXY} C_{nM} - L_{nATP} \quad (6)$$

$$\frac{dC_{aATP}}{dt} = 2k_{a3} C_E + 29 k_{aOXY} C_{aM} + 3 k_{GM} C_G - 3 k_{MG} C_{aM} - L_{aATP} \quad (7)$$

with L_{aATP} and L_{nATP} referring to the loss of ATP, i.e. energy demand, in astrocytes and neurons respectively.

Steady state

In the absence of CSD or other activation, glucose metabolism is in steady state, i.e. concentrations do not change with time. $C_{E,0}$ and $C_{L,0}$ were measured by rsMD and $K_{1,0}$, $k_{2,0}$ and $k_{3,0}$ were calculated from a 90-minute FDG PET scan in propofol anesthetized rats that were subjected to the same surgical procedures and where a cotton ball soaked in NaCl was applied for 70 minutes, causing no CSD waves (as verified by LSF). This sham experiment yielded $K_{1,0}$=0.072 ml/ml/min, $k_{2,0}$= 0.086 min^{-1}, and $k_{3,0}$=0.143

min^{-1}. Note that consistency between PET and rsMD was verified since C_E measured by rsMD was related to the plasma glucose level by $C_{E,0} = K_{1,0}/(k_{2,0} + k_{3,0})C_P$.

All other tissue concentrations were found in earlier reports[3] and intracellular concentrations for astrocytes and neurons were calculated given the neuron:astrocyte volume ratio according to:

$$C_{aM} = r_a C_M \quad (8)$$

$$C_{nM} = (1 - r_a) C_M \quad (9)$$

$$C_{aATP} = r_a C_{ATP} \quad (10)$$

$$C_{nATP} = (1 - r_a) C_{ATP} \quad (11)$$

Resulting concentrations are summarized in Supplementary Table S1. During baseline steady state conditions we assumed the following:

- astrocytes and neurons have the same capacity to fully oxidize glucose, i.e. $k_{aOXY,0} = k_{nOXY,0} = k_{OXY,0}$ [4]
- there is neither synthesis nor production of glycogen: $k_{MG,0} = k_{GM,0} = 0$
- there is a small amount of lactate transported from blood-stream to the brain: $k_{PL,0}$ [5]
- 100% of the lactate transported from blood into the brain are metabolized by neurons ($k_{nLM,0}C_{L,0}=k_{PL,0}C_P$)
- there is no consumption of lactate by astrocytes: $k_{aLM,0} = 0$
- the production rate of lactate is given by the fraction of energy production that is used for maintaining membrane resting potential, $P_{e,0}$, and therefore $k_{nML,0}=P_{e,0}k_{n3,0}C_{E,0}/C_{nM,0}$ and $k_{aML,0}=P_{e,0}k_{a3,0}C_{E,0}/C_{aM,0}$. According to Attwell and Laughlin, $P_{e,0}$ ~10 % of the total energy metabolism in grey matter of rats[6].
- consistent with a small net production of lactate the amount of lactate transported from blood to brain is 90% of the total amount of lactate produced by astrocytes and neurons: $k_{PL,0}C_P$=0.9 ($k_{nML,0}C_{nM,0}$+ $k_{aML,0}C_{aM,0}$)=0.9 $P_{e,0}$ ($k_{n3,0}$+ $k_{a3,0}$) $C_{E,0}$
- and that all of the lactate produced by astrocytes and neurons is removed: $k_{LP,0}C_{L,0}$= $P_{e,0}$ ($k_{n3,0}$+ $k_{a3,0}$) $C_{E,0}$

Thus all baseline steady state rate constants can be determined from the concentrations C_P, $C_{E,0}$, $C_{L,0}$, $C_{aM,0}$, $C_{nM,0}$ and the glucose rate constants $K_{1,0}$, $k_{2,0}$, $k_{a3,0}$, and $k_{n3,0}$ given the above assumptions and setting equations 1-4 to zero:

$$k_{PL,0} = 0.9P_{e,0}\frac{K_{1,0}(k_{a3,0}+k_{n3,0})}{k_{2,0}+k_{a3,0}+k_{n3,0}} \quad (12)$$

$$k_{LP,0} = P_{e,0}\frac{K_{1,0}(k_{a3,0}+k_{n3,0})}{k_{2,0}+k_{a3,0}+k_{n3,0}}C_P/C_{L,0} \quad (13)$$

$$k_{nLM,0} = k_{PL,0}C_P/C_{L,0} \quad (14)$$

$$k_{aLM,0} = 0 \quad (15)$$

$$k_{nML,0} = P_{e,0}\frac{K_{1,0}k_{n3,0}}{k_{2,0}+k_{a3,0}+k_{n3,0}}C_P/C_{nM,0} \quad (16)$$

$$k_{aML,0} = P_{e,0}\frac{K_{1,0}k_{a3,0}}{k_{2,0}+k_{a3,0}+k_{n3,0}}C_P/C_{aM,0} \quad (17)$$

$$k_{nOXY,0} = (1-P_{e,0})\frac{K_{1,0}k_{n3,0}}{k_{2,0}+k_{a3,0}+k_{n3,0}}C_P/C_{nM,0} + k_{PL,0}C_P/C_{nM,0} \quad (18)$$

$$k_{aOXY,0} = (1-P_{e,0})\frac{K_{1,0}k_{a3,0}}{k_{2,0}+k_{a3,0}+k_{n3,0}}C_P/C_{aM,0} \quad (19)$$

Resulting rate constants at steady state are summarized in Supplementary Table S2.

Response to energy challenge

Any changes in energy demand, i.e. any increases (or decreases) in the terms L_{aATP} and L_{nATP} in Eq. 6,7 will modify neuronal and astrocytic ATP concentrations. To respond to these changes, the rate constants must be adjusted, i.e. the rate constants are functions of C_{nATP} and C_{aATP}. We assume that the rate constants react to changes in ATP concentration in an exponential form because (1) it leads to stronger reactions in cases of very low ATP, i.e. critical ATP concentrations, (2) rate constants are not zero even at high concentrations of ATP, i.e. fluxes are never turned-off completely, and (3) for small changes of ATP concentration, the reaction linearly depends on ATP concentrations.

$$K_1 = K_{1,0}\exp\left\{f_1\left(1-\frac{C_{nATP}+C_{aATP}}{C_{nATP,0}+C_{aATP,0}}\right)\right\} \quad (20)$$

$$k_{x3} = k_{x3,0}\exp\left\{f_3\left(1-\frac{C_{xATP}}{C_{xATP,0}}\right)\right\} \quad (21)$$

$$k_{xOXY} = k_{xOXY,0}\exp\left\{f_{OXY}\left(1-\frac{C_{xATP}}{C_{xATP,0}}\right)\right\} \quad (22)$$

with indices 0 referring to the steady state values, and indices *x* referring to either astrocytes or neurons. We further assume that the ratio of inward and outward transport of glucose through the blood-brain barrier is kept constant, i.e. $K_1/k_2 = K_{1,0}/k_{2,0}$, and that K_1 cannot exceed a maximum value $K_{1,max} = 0.11$ mL/mL/min[7].

Furthermore, there is active removal of lactate to the blood, i.e. k_{LP} is a function of C_L:

$$k_{LP} = k_{LP,0} \exp\left\{-f_{LP}\left(1 - \frac{C_L}{C_{L,0}}\right)\right\} \quad (23)$$

Furthermore, lactate is taken-up by cells if the extracellular lactate level is elevated by more than 80% at stimulation. If turned on, this process continues until lactate returns to levels that only differ by <5% from normal levels.

$$k_{nLM} = k_{nLM,0} + \left(\exp\left\{f_{nLM}\left(1 - \frac{C_{nATP}}{C_{nATP,0}}\right)\right\} - 1\right)\min^{-1} \quad (24)$$

Finally, breakdown of glycogen is given by

$$k_{GM} = \left(\exp\left\{f_{GM}\left(1 - \frac{C_{aATP}}{C_{aATP,0}}\right)\right\} - 1\right)\min^{-1} \quad (25)$$

and reduction of glycogen content causes re-synthesis of glycogen[4]:

$$k_{MG} = \left(\exp\left\{f_{MG}\left(1 - \frac{C_G}{C_{G,0}}\right)\right\} - 1\right)\min^{-1} \quad (26)$$

All reaction factors, *f*, were determined by fitting the model output for C_E, C_L and FDG uptake to the experimental data (rsMD and PET). (See Supplementary Table S3)

Given these f factors, the rate constants (*k*'s) as functions of ATP concentration can be fully determined (see Supplementary Fig. S1).

Cellular membrane potential

Under normal conditions, all cells, including neurons and astrocytes, have an electrical potential difference across their membranes due to different intra- and extracellular ion concentrations established by energy demanding ion pumps. Neuronal firing causes short reductions of this polarization, which is re-established by increased activation of the ion pumps. Even in resting state, there is some neuronal activity and accordingly a certain fraction of cells has a decreased membrane potential. The total electrical potential energy in a volume of tissue is therefore slightly lower than the cell number in this volume times the resting potential energy. Increased activity changes the total polarization (or electrical potential energy). In order to describe the polarization status of ambient cells we assume that cells can only have two states: polarized and depolarized. The change in fractional number of polarized cells is then given by:

$$\frac{dn_p}{dt} = \frac{1}{\tau_r} n_{np} - \frac{1}{\tau_d} n_p \tag{27}$$

with n_p (n_{np}) is the fraction of (non-)polarized cells per volume. n_p can be either astrocytes or neurons with $n_{a,p} + n_{a,np} = r_a$ and $n_{n,p} + n_{n,np} = (1-r_a)$. In steady state, the number of cells that are polarized is then:

$$n_{n,p,0} = \frac{\tau_{d,0}}{\tau_{r,0} + \tau_{d,0}} (1 - r_a) \tag{28}$$

$$n_{a,p,0} = \frac{\tau_{d,0}}{\tau_{r,0} + \tau_{d,0}} r_a \tag{29}$$

With τ_r = 1.4 min and τ_d = 33 min, $n_{p,0}$ = 0.96. If the number of polarized cells is changed by an event like a spreading depression at t = 0, the solution of Eq. 27 describes how the number of polarized cells evolves with time:

$$n_p(t) = n_{p,0} \left(1 - e^{-\left(\frac{1}{\tau_r} + \frac{1}{\tau_d}\right)t}\right) + n_p(t=0) e^{-\left(\frac{1}{\tau_r} + \frac{1}{\tau_d}\right)t} \tag{30}$$

where $n_p(t = 0)$ is the number of polarized cells (astrocytes or neurons) at time zero after the event. Eq. 30 applies to astrocytes and neurons.

Energy metabolism for cell polarization per volume of tissue per time is proportional to the number of cells being polarized per time:

$$P_e(t) = E_0 \frac{1}{\tau_r} n_{np}(t) \tag{31}$$

In steady state this is:

$$P_{e,0} = \frac{E_0}{\tau_{r,0} + \tau_{d,0}} \tag{32}$$

We assume that the total energy metabolism per volume tissue and unit time can be divided into three parts, the electronic polarization energy P_e, an energy attributed to those processes that are shut down for a certain time after CSD P_x, and the rest P_{bg}. We normalize the energy, such that $P_{e,0}+P_{x,0}+P_{bg}$ =1. E_0 in Eq. 31, 32 is then

$$E_0 = \frac{1 - P_{x,0} - P_{bg}}{\tau_{r,0} + \tau_{d,0}} \tag{33}$$

From our data we propose the steady state energy contributions $P_{e,0}$ = 0.09 (Attwell and Laughlin 2001: 13% of total signaling energy, which is 75% of total cellular energy metabolism: ~10%[6]), $P_{x,0}$ = 0.23 (from the single SD FDG data), and P_{bg} = 0.68 accordingly.

Energy demand during CSD

Cortical spreading depression (CSD) causes an instant depolarization of all ambient cells ($n_p = 0$). It has further been shown that some cellular processes are shut down for a certain time after CSD ($P_x = 0$). We name the fraction of cells with $P_x = 0$ quiet cells, n_q. There are four groups of cells for astrocytes and neurons: 1. polarized and non-quiet $n_{p,nq}$, 2. non-polarized and quiet $n_{np,q}$, 3. polarized and quiet $n_{p,q}$, and 4. non-polarized and non-quiet $n_{np,nq}$.

We assume that the number of quiet cells after CSD is determined by the following equation:

$$\frac{dn_q}{dt} = -\frac{1}{t_q}\left(\frac{t - t_{CSD}}{t_q}\right)^{qex} n_q \tag{34}$$

when a CSD occurred at time t_{CSD}. This yields

$$n_q(t) = n_q(t_{CSD}) \exp\left\{-\frac{1}{qex+1}\left(\frac{t - t_{CSD}}{t_q}\right)^{qex+1}\right\} \tag{35}$$

Eq. 34 and 35 apply to neurons and astrocytes and have been constructed to have the following features: after being silenced from a CSD, cells remain quiet for a time t_q. Around time t_q after CSD cells return from quiet to non-quiet state. *qex* determines the time scale for this transition. We set $t_q = 55$ min (duration of negative slope in the FDG curve (ipsilateral-contralateral) after single CSD) and $qex = 12$ (see Supplementary Fig. S2).

We assume that only polarized cells are influenced by a CSD. A CSD instantly depolarizes and silences all polarized cells. Non-polarized cells are not affected by the CSD. Since the time for the transition from quiet to non-quiet state depends on the time when these cells have been depolarized, cells have to be assigned to a certain CSD. At the time point the *i*th CSD hits the cells, the cell numbers are reorganized for astrocytes and neurons in the following way:

$$n_{np,q,i} = \sum_{j=0}^{i-1} n_{p,nq,j} + n_{p,q,j} \tag{36}$$

$$n_{p,q,j} = 0 \qquad (j = 0 \ldots i) \tag{37}$$

$$n_{p,nq,j} = 0 \qquad (j = 0 \ldots i) \tag{38}$$

The cell numbers then change in time according to Eq. 27, 30, 34, and 35. The total cell numbers after *i* CSDs are then given by:

$$n_{p,q}(t) = \sum_{j=0}^{i} n_{p,q,j}(t) \quad (39)$$

$$n_{np,q}(t) = \sum_{j=0}^{i} n_{np,q,j}(t) \quad (40)$$

$$n_{p,nq}(t) = \sum_{j=0}^{i} n_{p,nq,j}(t) \quad (41)$$

$$n_{np,nq}(t) = \sum_{j=0}^{i} n_{np,nq,j}(t) \quad (42)$$

for astrocytes and neurons. For calculation of the energy metabolism, cell numbers are regrouped into polarized n_p, non-polarized n_{np}, quiet n_q and non-quiet n_{nq} cells by:

$$n_p(t) = n_{p,q}(t) + n_{p,nq}(t) \quad (43)$$

$$n_{np}(t) = n_{np,q}(t) + n_{np,nq}(t) \quad (44)$$

$$n_q(t) = n_{p,q}(t) + n_{np,q}(t) \quad (45)$$

$$n_{nq}(t) = n_{p,nq}(t) + n_{np,nq}(t) \quad (46)$$

Now we can calculate the impact of a CSD on local energy metabolism, which is altered in two ways: 1. by increasing the number of non-polarized cells the energy for electronic polarization is elevated (Eq. 31), 2. by silencing the fraction P_x of the normal energy metabolism (Supplementary Fig. S2). Energy metabolism at time t is then given by:

$$P_{tot}(t) = P_e(t) + P_x(t) + P_{bg} \quad (47)$$

with

$$P_e(t) = E_0 \left(\frac{n_{a,np}(t)}{\tau_{a,r}} + \frac{n_{n,np}(t)}{\tau_{n,r}} \right) \quad (48)$$

$$P_x(t) = \left(1 - n_{a,q}(t) - n_{n,q}(t)\right) P_{x,0} \quad (49)$$

In order to ensure that energy metabolism cannot exceed the available amount of energy in terms of ATP, the polarization times τ_r are functions of the ATP concentration. Since ATP levels in astrocytes and neurons can differ after neuronal activation, the polarization times for astrocytes and neurons can be different:

$$\tau_{n,r} = \tau_r \frac{C_{nATP,0}}{C_{nATP}} \quad (50)$$

$$\tau_{a,r} = \tau_r \frac{C_{aATP,0}}{C_{aATP}} \quad (51)$$

At low levels of ATP it takes longer to polarize the cells. Inserting Eq. 50 and 51 into Eq. 48, the power of the ion pumps, P_e, is proportional to ATP concentration. In the absence of ATP, ion pumps do not work (P_e=0).

The timings of energy challenges caused by the CSD waves were determined by LSI imaging and served as input to the model.

Supplementary Material S2 – Comparison of model output with experimental data

Theoretical model and rsMD data

Our multimodal experimental setup enables us to measure $C_{E,MD}$ and $C_{L,MD}$ (by rsMD), and FDG uptake (by PET) at all times.

However, rsMD glucose and lactate concentrations are extracellular concentrations modified by MD sampling recovery and by dispersion along the connection tubing. If we assume a steady recovery during the whole procedure, then rsMD concentration *changes* are equal to extracellular concentration *changes* (Fig. 1b-c-d). We determined the dispersion effect of the tubing by *in vitro* experiments using the same setup and applied dispersion and recovery to model-derived extracellular glucose and lactate concentrations for comparison with the measured data in the following way:

Recovery:

$$C_{MD}(t) = k_{MD}\int_{t-t_{MD}}^{t} dt' C_{EC}(t') e^{-k_{MD}(t-t')} \tag{52}$$

$$\frac{dC_{MD}}{dt} = k_{MD}(C_{EC}(t) - C_{MD}(t)) - k_{MD}e^{-k_{MD}t_{MD}}C_{EC}(t-t_{MD}) \tag{53}$$

t_{MD} is the time for a volume element to propagate along the membrane of the micro dialysis (given by the flow rate and membrane volume), and therefore the time available for molecules to diffuse in and out of the membrane. Here, for the microdialysis probe MAB 6.14.2 perfused at 1.6µL/min, t_{MD}=0.35min. k_{MD} is the effective diffusion coefficient for lactate and glucose through tissue, membrane and dialysate. k_{MD} was determined *in vivo* using Eq. 53 in steady state and stopping dialysate flow for three minutes to obtain C_{EC}, yielding k_{MD} = 0.14 min^{-1}.

Dispersion:

Dispersion through tubing from MD membrane to rsMD measurement is described by the following equation:

$$C_{rsMD}(t) = \int_0^{\tau} dt' C_{MD}(t-t') f_{disp}(t') \tag{54}$$

We chose an exponential dispersion function. Mass conservation requires the integral over the dispersion function to be equal to 1 yielding

$$f_{disp}(t) = \frac{k_{disp}}{1 - e^{-k_{disp}\tau}} e^{-k_{disp}t} \tag{55}$$

The measured concentrations are then related to the concentrations of the dialysate at the MD probe by:

$$C_{rsMD}(t) = \frac{k_{disp}}{1 - e^{-k_{disp}\tau}} \int_{t-\tau}^{t} dt' C_{MD}(t') e^{-k_{disp}(t-t')} \tag{56}$$

$$\frac{dC_{rsMD}}{dt} = \frac{k_{disp}}{1 - e^{-k_{disp}\tau}} \left[C_{MD}(t) - e^{-k_{disp}\tau} C_{MD}(t-\tau) \right] - k_{disp} C_{rsMD}(t) \tag{57}$$

The C_{rsMD} curves calculated from the extracellular lactate and glucose concentrations using Eq. 52, 53, 56, and 57 can be compared with measured rsMD data. We used the following parameters for dispersion $\tau = 11$ min (time delay due to tubing), and $k_{disp} = 0.5$ min^{-1}. k_{disp} was determined from in vitro recovery experiments, performed before the animal experiment: the MD probe was put in 5 mM and we measured rsMD with the same tubing as during animal experiments.

Theoretical model and FDG-PET data

FDG is analogue to glucose but it is trapped in the cells after being phosphorylated to FDG-6-phosphate. The glucose transporters and the hexokinase have different efficiencies for transporting and phosphorylating FDG compared to glucose. These differences are universal and have been measured by Haselbalch et al.[8,9]: $L_1 = K_1^*/K_1 = 1.48$ and $L_3 = k_3^*/k_3 = 0.38$. Given the rate constants K_1^*, k_2^*, and k_3^*, and the input function of FDG $C_P^*(t)$, the uptake of FDG in tissue at time t+Δt after tracer injection is given by:

$$C_E^*(t+\Delta t) = C_E^*(t) e^{-(k_2^*+k_3^*)\Delta t} + K_1^* \int_t^{t+\Delta t} dt' C_P^*(t') e^{-(k_2^*+k_3^*)(t+\Delta t-t')} \tag{58}$$

$$C_M^*(t+\Delta t) = C_M^*(t) + k_3^* \int_t^{t+\Delta t} dt' C_E^*(t') \tag{59}$$

$$C_T^*(t+\Delta t) = C_E^*(t+\Delta t) + C_M^*(t+\Delta t) \tag{60}$$

with $C_T^*(0)=C_E^*(0)=C_M^*(0)=0$. As input function $C_P^*(t)$ we used an average from directly measured input function in rats that were injected in the same way[10]. Since all data are normalized by the contralateral hemisphere, the absolute scaling of the input function is not influencing the comparison of model output and measured data.

Given the rate constants K_1, k_2, and k_3 for glucose as a function of time from the output of the model, the rate constants for FDG as a function of time are $K_1^* = L_1K_1$, $k_2^* = L_1k_2$, and $k_3^* = L_3k_3$. FDG uptake can then be calculated using Eq. 58, 59, and 60 with sufficiently small time intervals Δt to assume

constant rate constants during each time interval. This calculated FDG uptake curve was used to compare model output with measured FDG data.

Time of CSD occurrence

Number of CSDs and time intervals between consecutive CSDs were determined from LSI imaging, where CSDs can be detected as hyperemic waves at a temporal resolution of < 1s. To compare data from multiple CSDs with the model, time intervals from the seven animals in multiple-CSD-group were averaged (Fig. 1c).

Supplementary Material S3 - Energy metabolism during CSD

During CSD all ambient cells – astrocytes and neurons – are depolarized and the following repolarization causes an increase in energy metabolism and a related increase in CBF[7,11,12]. After repolarization, CBF drops below baseline and oligemia persists for a period of ~1 hour (Fig. 1d)[12,13] while extracellular glucose remains significantly decreased (Fig. 1d)[14]. During this time we observe a decreased uptake of FDG: the difference to the control hemisphere gradually disappears (Fig. 1, d). Low extracellular glucose levels and subnormal uptake of FDG are consistent with decreased energy metabolism (Fig. 1b). Thus, it seems that certain energy demanding cellular processes (P_x in our model) are impaired for ~1 hour after a single CSD (Supplementary Fig. S3). This may seem counter-intuitive, but previous experimental data do support this finding. The autoradiograms of Shinohara et al.[11] also show slightly reduced 14C-deoxyglucose uptake during this period in conscious rats. Guiou et al. [15] observed significantly reduced integrated response to somatosensory evoked potential in enflurane anesthetized rats up to 60 minutes post CSD, suggesting that some energy demanding processes are indeed silenced for so long. This is however in contradiction to Piilgaard et al.[12], who observed an increased oxygen consumption rate during this phase in alpha-chloralose anesthetized rats. Furthermore, Lauritzen and Diemer[16] report no significant differences in CMR_{glc} between ipsi- and contralateral hemisphere in halothane anesthetized rats when the tracer was injected fifteen minutes after the CSD had traversed the cortex. However, as discussed by Backes et al.[10] preservation of CMR_{glc} at decreased unidirectional influx of glucose (due to a reduction of blood flow) leads to an increase in net deoxyglucose uptake synonymous to changes in the lumped constant. Preserved deoxyglucose uptake would then be consistent with reduced CMR_{glc}.

Supplementary Material S4 – Perturbation of steady state concentrations

In order to test robustness of the model each substrate concentration was set to its double steady state value at time 0. Running the model, the time until the system returned to steady state was determined (time t when $|C(t)-C_0|/C_0<0.01$). Times are listed in Supplementary Table S4.

Note that the time scale to refill glycogen is very long but of the same order of magnitude as measured by Krivanek (J Neurochemistry, 1958)[17].

This shows that, even with drastic variations in concentrations, the model converges to steady state conditions within a reasonable time, indicating robustness.

Supplementary Material S5 – Brain metabolism under propofol anesthesia

We chose propofol as anesthetic agent because in comparison to other anesthetic agents metabolism under propofol is not so different from the awake state.

Matsumura et al.[18] compared glucose metabolism in rats under different anesthetic agents and in the awake state. Propofol anesthesia clearly shows the most similar (though reduced) distribution of glucose metabolism in comparison to the awake state.

In our lab, we monitored changes in blood flow in rats when switching from isoflurane to propofol anesthesia[19] and saw a reduction of baseline CBF under propofol. This difference in baseline CBF from propofol to isoflurane was in the same order of magnitude as that measured from unanesthetized to isoflurane[20].

Oshima et al.[21] analyzed blood flow and $CMRO_2$ under propofol in humans and stated: "…normal cerebral circulation and metabolism are maintained." We therefore concluded that CMRglu, CBF and CMRO2 in the awake state were comparable to our conditions under propofol.

Ori et al.[22] found: "Propofol, at all the doses tested, did not alter the concentrations of adenine nucleotides, phosphocreatine, lactate, pyruvate, or glucose in normoxic rats."

Supplementary Material S6 – Variation of volume ratio

For our model we assumed that (1) the metabolically active cells can be effectively divided into two groups: astrocytes and neurons and (2) that under baseline conditions astrocytes contribute 36% to the tissue volume covered by metabolically active cells and neurons 64% (r_a=0.36). Since this value is not well substantiated with measured data, we re-calculated the model with r_a=0.2 and r_a=0.7. Results of substrate concentrations after CSD in comparison to the case of r_a=0.36 are shown in Supplementary Figure S4. Although the values of 0.2 and 0.7 span a wide range there is only small variations in the total metabolic response to CSD, which is presumably due to the fact that during CSD *all* cells are depolarized and require energy for repolarization. But there are clear differences in the contributions of each cell type to overall metabolic response.

Supplementary Figures

Supplementary Figure S1

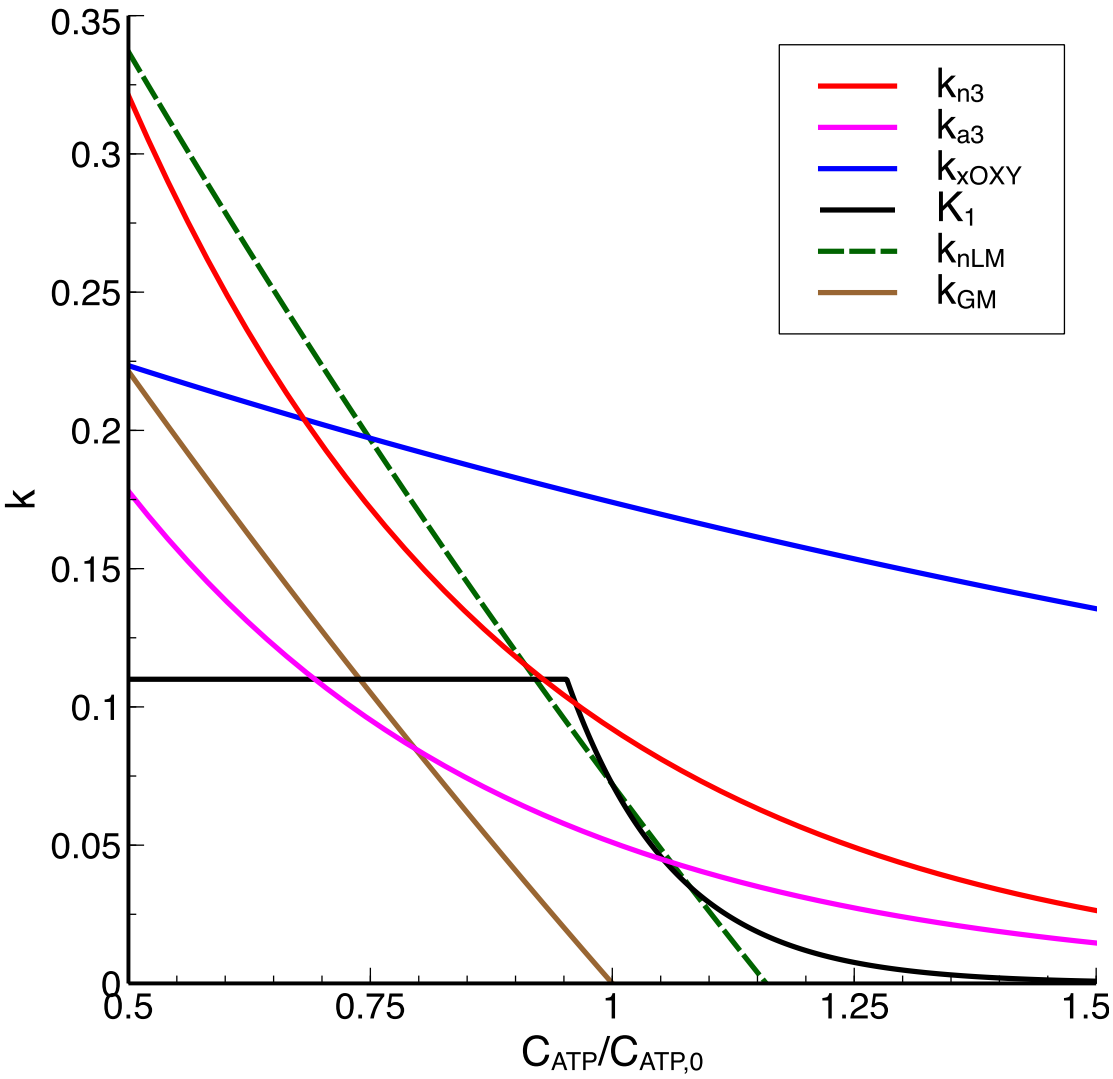

Rate constants as functions of cellular ATP levels.

Supplementary Figure S2

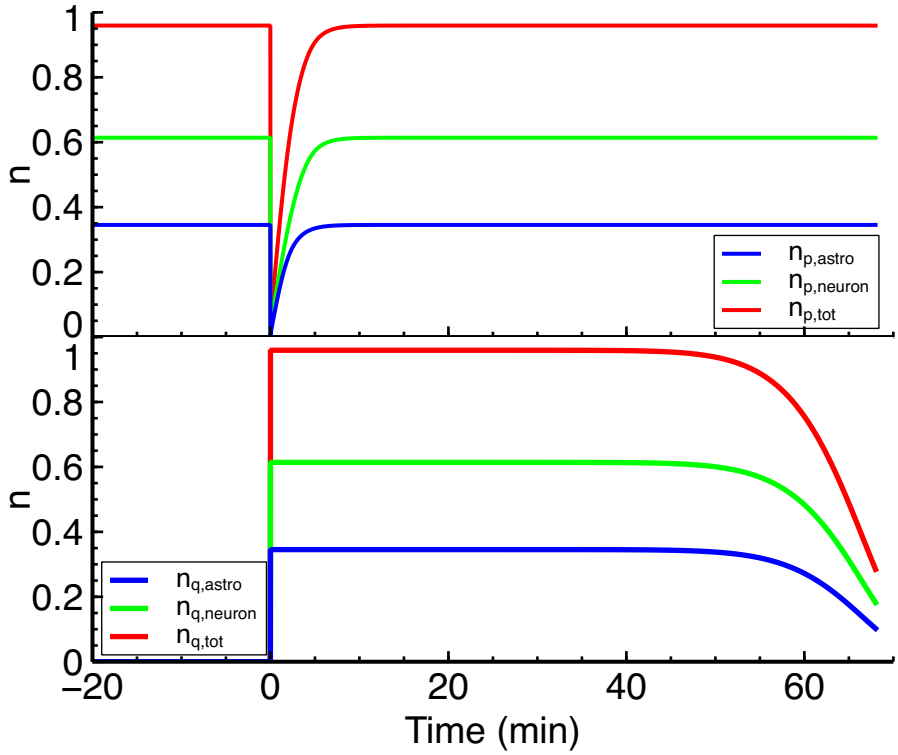

Fractional cell numbers as function of time after single CSD.

Supplementary Figure S3

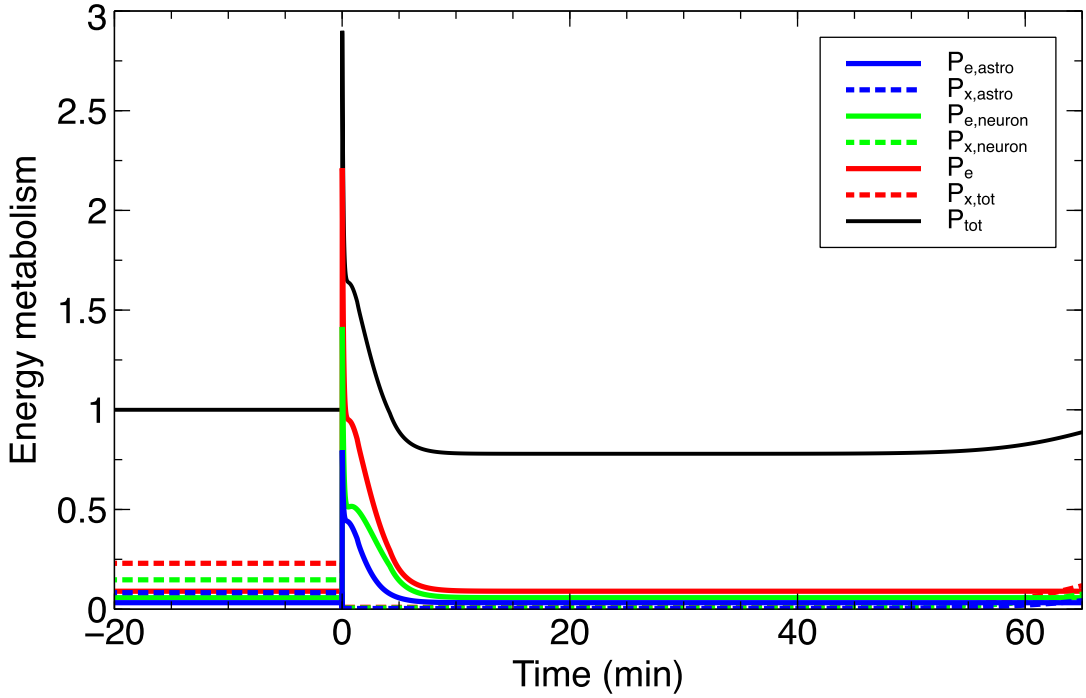

Energy metabolism after single CSD in fractions baseline energy metabolism.

Supplementary Figure S4

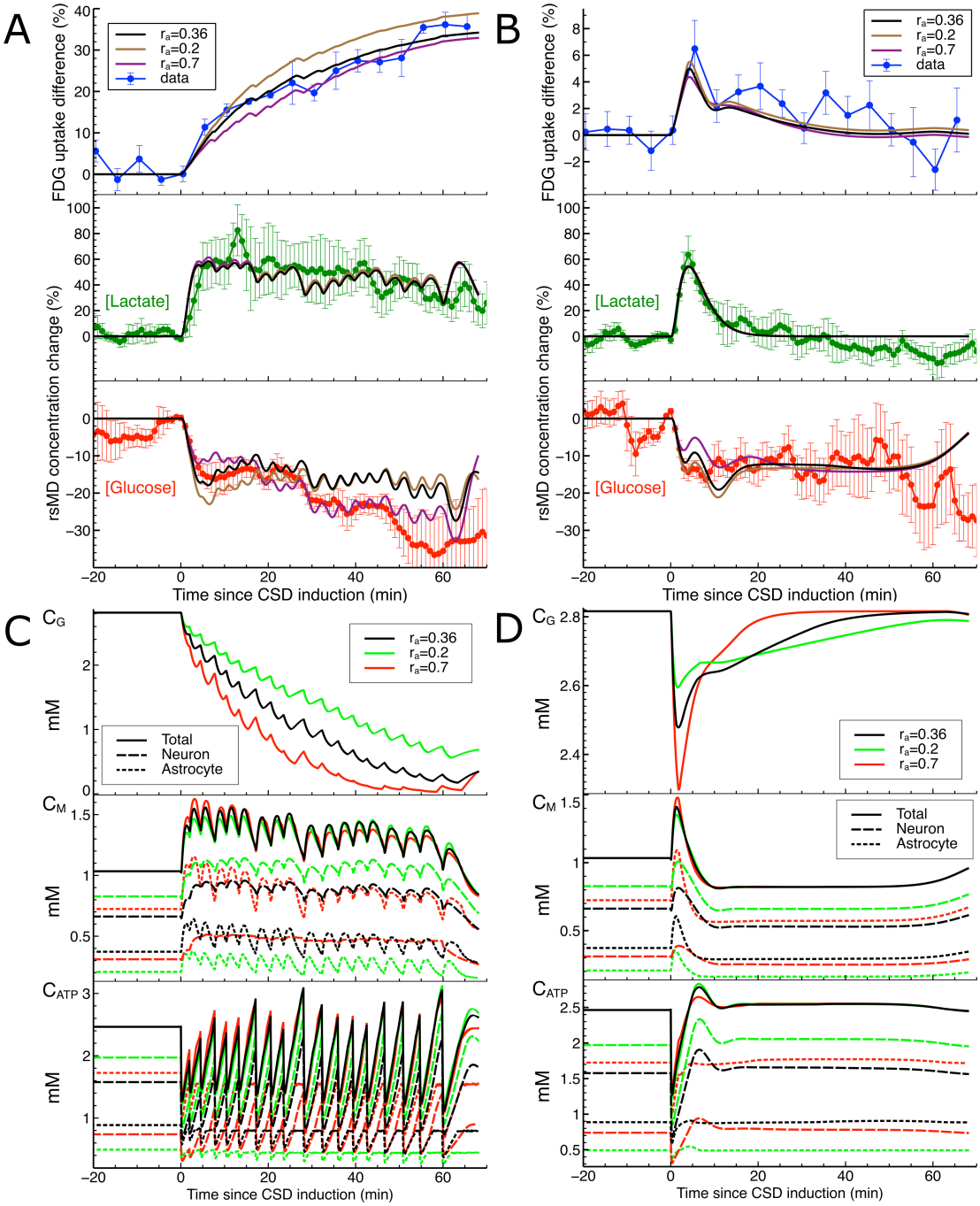

Substrate concentrations in response to CSD as output from the model for different values of the astrocytic volume ratios r_a. A, B show model results in comparison to the measured data (see main text). C, D show results for C_G, C_M, C_{ATP}. The different colors indicate different values of r_a and the line type (solid, long dashed, short dashed) the cell type.

Supplementary Tables

Supplementary Table S1 – Steady state concentrations

Substance	Fraction of C_P	[mM]	Reference
C_P	1.000	4.4	[1]
C_E	0.315	1.39	[1,2]
C_L	0.050	2×0.22	[1,3]
C_G	0.640	2.8	[4]
C_{nM}	0.150	0.66	[4]
C_{aM}	0.085	0.37	[4]
C_{nATP}	0.358	1.58	[4]
C_{aATP}	0.202	0.89	[4]

[1] Measurements in n=15 animals included in the study (for plasma glucose) or in sham animal (extracellular concentrations), [2] Di Nuzzo et al. (2010)[23], [3] Cloutier et al. (2009)[24], [4] Hawkins et al. (1973)[3].

Supplementary Table S2 – Steady state rate constants

Rate constant	Value	Units
$K_{1,0}$	0.072	ml/ml/min
$k_{2,0}$	0.086	min^{-1}
$k_{n3,0}$	0.092	min^{-1}
$k_{a3,0}$	0.051	min^{-1}
$k_{nOXY,0}$	0.174	min^{-1}
$k_{aOXY,0}$	0.174	min^{-1}
$k_{nML,0}$	0.017	min^{-1}
$k_{aML,0}$	0.017	min^{-1}
$k_{nLM,0}$	0.072	min^{-1}
$k_{aLM,0}$	0	min^{-1}
$k_{LP,0}$	0.081	min^{-1}
$k_{PL,0}$	0.004	min^{-1}

Supplementary Table S3 – Parameters that control the response to changes in cellular ATP levels

$K_{1,max}$	0.11 mL/mL/min
f_1	9.00
f_3	2.50
f_{OXY}	0.50
f_{nLM}	0.47
f_{aLM}	0.00
f_{GM}	0.40

Supplementary Table S4 – Time to reach steady state conditions

Perturbed concentration	Time to return to steady state [min]
C_E	10.78
C_L	11.90
C_{aM}	10.22
C_{nM}	62.43
C_{aATP}	16.84
C_{nATP}	7.55
C_G	160

See Supplementary Material S4 for description.

References – Supplementary Information

1 Mangia S, DiNuzzo M, Giove F, Carruthers A, Simpson IA, Vannucci SJ. Response to “comment on recent modeling studies of astrocyte-neuron metabolic interactions”: much ado about nothing. *J Cereb Blood Flow Metab* 2011; **31**: 1346–53.

2 Pfeuffer J, Tkác I, Gruetter R. Extracellular-intracellular distribution of glucose and lactate in the rat brain assessed noninvasively by diffusion-weighted 1H nuclear magnetic resonance spectroscopy in vivo. *J Cereb Blood Flow Metab* 2000; **20**: 736–46.

3 Hawkins RA, Miller AL, Nielsen RC, Veech RL. The acute action of ammonia on rat brain metabolism in vivo. *Biochem J* 1973; **134**: 1001–8.

4 Hertz L, Peng L, Dienel GA. Energy metabolism in astrocytes: high rate of oxidative metabolism and spatiotemporal dependence on glycolysis/glycogenolysis. *J Cereb Blood Flow Metab* 2007; **27**: 219–49.

5 Van Hall G, Strømstad M, Rasmussen P, Jans O, Zaar M, Gam C, *et al.* Blood lactate is an important energy source for the human brain. *J Cereb Blood Flow Metab* 2009; **29**: 1121–9.

6 Attwell D, Laughlin SB. An energy budget for signaling in the grey matter of the brain. *J Cereb Blood Flow Metab* 2001; **21**: 1133–45.

7 Gjedde A, Hansen AJ, Quistorff B. Blood-brain glucose transfer in spreading depression. *J Neurochem* 1981; **37**: 807–12.

8 Hasselbalch SG, Knudsen GM, Holm S, Hageman LP, Capaldo B, Paulson OB. Transport of D-glucose and 2-fluorodeoxyglucose across the blood-brain barrier in humans. *J Cereb Blood Flow Metab* 1996; **16**: 659–66.

9 Hasselbalch SG, Madsen PL, Knudsen GM, Holm S, Paulson OB. Calculation of the FDG lumped constant by simultaneous measurements of global glucose and FDG metabolism in humans. *J Cereb Blood Flow Metab* 1998; **18**: 154–60.

10 Backes H, Walberer M, Endepols H, Neumaier B, Graf R, Wienhard K, *et al.* Whiskers area as extracerebral reference tissue for quantification of rat brain metabolism using (18)F-FDG PET: application to focal cerebral ischemia. *J Nucl Med* 2011; **52**: 1252–60.

11 Shinohara M, Dollinger B, Brown G, Rapoport S, Sokoloff L. Cerebral glucose utilization: local changes during and after recovery from spreading cortical depression. *Sci (New York, NY)* 1979; **203**: 188–90.

12 Piilgaard H, Lauritzen M. Persistent increase in oxygen consumption and impaired neurovascular coupling after spreading depression in rat neocortex. *J Cereb Blood Flow Metab* 2009; **29**: 1517–27.

13 Lauritzen M, Jørgensen MB, Diemer NH, Gjedde A, Hansen AJ. Persistent oligemia of rat cerebral cortex in the wake of spreading depression. *Ann Neurol* 1982; **12**: 469–74.

14 Mies G, Paschen W. Regional changes of blood flow, glucose, and ATP content determined on brain sections during a single passage of spreading depression in rat brain cortex. *Exp Neurol* 1984; **84**: 249–58.

15 Guiou M, Sheth S, Nemoto M, Walker M, Pouratian N, Ba A, *et al.* Cortical spreading depression produces long-term disruption of activity-related changes in cerebral blood volume and neurovascular coupling. *J Biomed Opt* 2005; **10**: 11004.

16 Lauritzen M, Diemer NH. Uncoupling of cerebral blood flow and metabolism after single episode of cortical spreading depression in the rat brain. *Brain Res* 1986; **370**: 405–8.

17 Krivanek J. Changes of brain glycogen in the spreading EEG-depression of Leao. *J Neurochem* 1958; **2**: 337–43.

18 Matsumura A, Mizokawa S, Tanaka M, Wada Y, Nozaki S, Nakamura F, *et al.* Assessment of microPET performance in analyzing the rat brain under different types of anesthesia: comparison between quantitative data obtained with microPET and ex vivo autoradiography. *Neuroimage* 2003; **20**: 2040–50.

19 Feuerstein D, Takagaki M, Gramer M, Manning A, Endepols H, Vollmar S, *et al.* Detecting tissue deterioration after brain injury: regional blood flow level versus capacity to raise blood flow. *J Cereb Blood Flow Metab* 2014; **34**: 1117–27.

20 Sicard K, Shen Q, Brevard ME, Sullivan R, Ferris CF, King JA, *et al.* Regional Cerebral Blood Flow and BOLD Responses in Conscious and Anesthetized Rats Under Basal and Hypercapnic Conditions[colon] Implications for Functional MRI Studies. 2003; **23**: 472–81.

21 Oshima T, Karasawa F, Satoh T. Effects of propofol on cerebral blood flow and the metabolic rate of oxygen in humans. *Acta Anaesthesiol Scand* 2002; **46**: 831–5.

22 Ori C, Cavallini L, Freo U, Ruggero S, Ermani M, Pizzolato G, *et al.* The effects of propofol on cerebral high energy metabolites, lactate, and glucose in normoxic and severely hypoxic rats. *Life Sci* 1997; **60**: 1349–57.

23 DiNuzzo M, Mangia S, Maraviglia B, Giove F. Glycogenolysis in astrocytes supports blood-borne glucose channeling not glycogen-derived lactate shuttling to neurons: evidence from mathematical modeling. *J Cereb Blood Flow Metab* 2010; **30**: 1895–904.

24 Cloutier M, Bolger FB, Lowry JP, Wellstead P. An integrative dynamic model of brain energy metabolism using in vivo neurochemical measurements. *J Comput Neurosci* 2009; **27**: 391–414.